A DEEP LEARNING APPROACH WITH UNCERTAINTY ESTIMATION TO ASSESSMENT THE POTENTIAL OF ABOVEGROUND BIOMASS MAPPING OF TROPICAL RAINFOREST IN THAILAND

Songphon Reangsang, Suwit Navakam, Poramate Manoonpong, Anuphao Aobpaet, Pasuta Sunthornhao, Natnicha Yooyen, Sasawat Soontaros, and Soravis Supavetch*

songphonr@varuna.co.th, suwit.n@pttplc.com, poramate.m@vistec.ac.th, fengaha@ku.ac.th, fforpts@ku.ac.th, natnicha_y@pttplc.com, sasawat.s@pttplc.com, fengsvsu@ku.ac.th*

ABSTRACT

This study aims to develop an aboveground biomass density model by fusing spaceborne remote sensing data including Sentinel-1, Sentinel-2, and GEDI, with a U-Net convolutional neural network to overcome the limitation of sparse data coverage in Thailand and scale at the national level. Tropical rainforests and other forested areas such as perennial crop regions with similar geographical characteristics were evaluated by the models. Five models were developed using a deep ensemble technique to provide uncertainty estimation, and accuracy was validated using three types of forest inventory data. Results show high uncertainty in the out-of-distribution data areas, with %RRMSE for Pará rubber, mixed deciduous forest, and dry evergreen forest of 17.05, 24.47, and 14.0, respectively.

Index Terms **-** Aboveground Biomass; Carbon Stock; Tropical Rainforest; Deep Learning; CNN; U-Net

1. INTRODUCTION

While traditional field inventory methods reliably estimate forest biomass, remote sensing is emerging as a practical alternative for covering large areas, thereby reducing costs, manpower requirements, and project duration. However, it is crucial to ensure accuracy of remote sensing methodology compared to standard methods and this issue remains largely unaddressed in Thailand. AGB correlates directly to the physical characteristics of forests and plant species [1]. These relations lead to equations in AGB estimation that vary across different environmental areas. The objective of this study is to develop models that imitate the allometric equations of various reported studies targeting forest types in Thailand, covering all forms of allometric equations within a single model using remote sensing data. However, the correlation between forest features and the spectral characteristics of wave data obtained from remote sensing data is complex and not yet proven on their interrelation [2]. Using only data from multispectral imagery or radar imagery may not be sufficient for model development. In contrast, LiDAR data directly offers high-resolution physical information on forests. Through continuous advancements in technology, GEDI Mission by NASA, which utilizes satellite LiDAR with highest precision to this date, provides footprint-level forest structures [3]. Nevertheless, limitations persist in terms of spatial resolution and data measurement frequency, covering only a mere 4% of the earth's surface and the sparse data coverage in Thailand possess a challenge for its applicability [3]. Missions such as Sentinel-2 and Sentinel-1 have been extensively reported for their potential in building models to estimate AGB density value [4]. Although both datasets do not directly assess the physical structure of forests, these two satellites have a high spatial-resolution and extensive coverage of the earth's surface with higher measurement frequency. Therefore, the idea emerged to merge GEDI data with multispectral imagery or radar imagery, resulting in overcoming limitations of each dataset [5]. Due to the substantial quantity of satellite image data available, using deep learning methods for model development has been preferred. Deep learning models can extract pertinent features to formulate equations in assessing AGB from raw data trained by incorporating combined data from Sentinel-1, Sentinel-2, and GEDI. Previous studies have indicated success in evaluating forest structures or AGB using satellite-based remote sensing data [4] [6].

2. MATERIALS AND METHODS

2.1 Inventory Data Collection and AGB Estimation

With regards to the types of tropical rainforest, three study areas involved in this study were mixed deciduous forest in Nakhon Sawan, dry evergreen forest in Nakhon Ratchasima, and para rubber (*Hevea brasiliensis*) plantation in Rayong. Ground data were collected from randomly selected sample plots of 100x100 m, 3 plots (3 replicates) for each forest type. Sub-plots of 10x10 m were placed within the sample plots, which were placed in the north-south direction corresponding to the satellite imagery grid. Only trees with a height (H) of not less than 130 centimeters and a diameter at breast height (DBH) of not less than 4.5 centimeters were considered in this study. Trees in each plot were measured for DBH in centimeters (cm) and H in meters (m) and this dataset was used in the allometry equations to calculate AGB. The

equations of Ogawa et.al. (1965) [7], and Tsutsumi et.al. (1983) [8], and Hytönen et.al. (2018) [9] were applied to calculate AGB for mixed deciduous forest, dry evergreen forest, and rubber plantation, respectively. The amount of carbon storage in tree biomass was assessed using the IPCC (2006) conversion factor of 0.47. Finally, the amount of carbon dioxide absorbed was evaluated by multiplying the ratio of CO_2 to C (44:12*)* to the amount of carbon stored.

2.2 Data for Model Development

2.2.1. Sentinel-2

Data obtained from the multispectral instrument (MSI) Level-2A for both Sentinel-2A and Sentinel-2B encompasses 12 bands—namely B1, B2, B3, B4, B5, B6, B7, B8, B8A, B9, B11, and B12. These bands cover the period from November 1, 2020, to April 30, 2021, aiming to ensure uniform physical characteristics of forest canopy height. These data are utilized as predictor variables in the model. Due to the sensor's inability to capture data through clouds, satellite images are prepared by filtering out images with more than 50% cloud coverage using the QA60 data, a cloud mask image [10]. Then, a time series was selected as median composite to eliminate data variation between day and night to obtain the clearest cloud-free images before processing [4]. Images were normalized to a 0-1 scale to expedite model training and improve model accuracy [11]. Finally, images at different spatial resolutions (10 m, 20 m, and 60 m) were resampled to 50 m.

2.2.2. Sentinel-1

Utilizing data within the same temporal range as Sentinel-2 (November 1, 2020, to April 30, 2021), since Sentinel-1B ceased its mission during this period, Sentinel-1A data was used instead in Ground Range Detected (GRD) Interferometric Wide Swath (IW) mode. This data includes Vertical-Vertical (VV) and Vertical-Horizontal (VH) polarizations. It has been reported that this system can penetrate clouds and demonstrated capability in forest biomass assessment [12]. Hence, it was integrated with Sentinel-2 data as predictor variables. Data was preprocess using the Google Earth Engine (GEE) platform and the Sentinel-1 Toolbox, involving steps like thermal noise removal, radiometric calibration, and terrain correction. The data was normalized to a range of -30 to 0 decibels (dB) and a median composite was applied to all images in the selected timeframe. Eventually, normalization to a 0-1 scale and resampling spatial resolution to 50 m was performed to be consistent with Sentinel-2 imagery.

2.2.3. GEDI

The Global Ecosystem Dynamics Investigation (GEDI) mission is the first satellite with LiDAR survey capabilities that is designed for forest structure assessment. It provides high spatial resolution data with 25 m footprint diameter and spaced 60 m apart. The measurement lines are 600 m apart, Data was processed into different levels, such as L2A to estimate canopy height and L4A showing ABG data with global-scale accuracy coverage. For this development, GEDIv002 L4A data, refined for horizontal accuracy to 10 m, was utilized to serve as the reference ground truth for model development [13]. To ensure the highest quality and completeness of the data, certain data filtering criteria were applied as Data not meeting the quality requirement of L4 level : (l4_quality_flag = 0) [13] [14], unreliable data with a relative standard error in AGB exceeding 50% : ((agbd_se/agbd) x 100) > 50 [15], Data within sloped terrain areas exceeding 30% determined using NASA's Shuttle Radar Topography Mission (SRTM) Digital Elevation Model (DEM) for slope calculations [16], Data sourced from regions beyond the forested areas using WorldCover 2021 soil coverage data from ESA, categorized into various types: Built-up, Sparse vegetation, Snow and Ice, Permanent water bodies, Herbaceous wetland, Moss and lichen [15] [17], Data in areas with a degraded forest landscape or sparse vegetation using EO tree cover data from Landsat satellites in 2000 and 2010 from NASA and filtering out areas with less than 30% forest cover [17], and Data in the area which has NDVI lower than 0.3 [17]. Due to GEDI data's horizontal geospatial accuracy of ±10 m, which may introduce errors when directly used with other remote sensing data[18], the spatial resolution was resampled to 50 m using an aggregation technique to improve accuracy. The aggregation involves calculating the average value of GEDI data that have more than 1 sample within the target pixel size of 50 m. As illustrated in Fig. 1 [15]. The entire set of GEDI data covers the temporal range from November 1, 2020, to April 30, 2021.

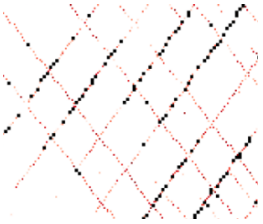

Fig. 1. GEDI raster image at a spatial resolution of 25 m (red) and GEDI raster image at a spatial resolution of 50 m (black)

2.3 Accuracy Assessment of GEDI Satellite Imagery

Quantitative method was use in this study to compares the error values of remote sensing data and field inventory data. Due to the sparse-pattern, lack of coverage in GEDI data points and the limited accessibility of inventory data samples, spatial misalignment of the two datasets might occur, hence, they cannot be directly compared. Therefore, geostatistical techniques are implemented to interpolate missing GEDI. Value in the area close to GEDI data points was predicted by considering the surrounding spatial characteristics [19]. Since GEDI has data distribution that covers the uniformly entire study area, a spatial interpolation technique which is ordinary kriging was applied as the analysis formula. Geostatistical analysis was conducted using the QGIS-LTR program (version 3.28) and the Smart-map plugin (version 1.3.2) [20]

was used to automatically identify suitable parameters to fit the model for each study area. Sample interpolation results are illustrated in Fig. 2.). The quantitative comparison results between GEDI data and field data are shown in Fig. 3.

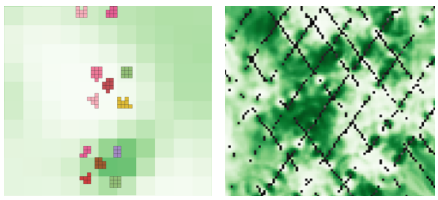

Fig. 2. Aboveground biomass density $[kg/m^2]$
(a) sample in Rayong area compared to inventory data
(b) sample Rayong area compared to GEDI 50 m footprint

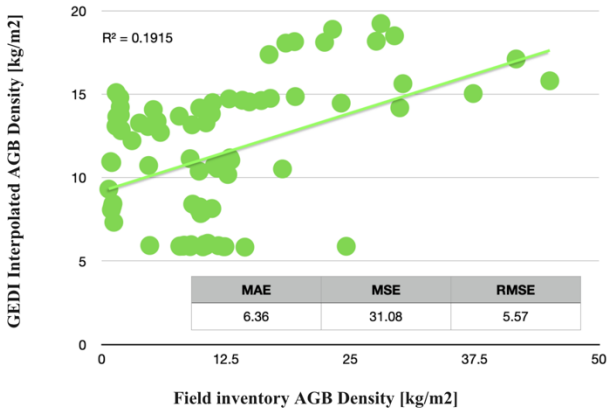

Fig. 3. Results comparison between GEDI AGB density accuracy assessment and inventory data

2.4 Methodology

The model uses data from satellite-based remote sensing to infer the AGB value at each pixel. This technical approach known as Pixel-wise regression. U-Net, a convolutional neural network (CNN) known for its proficiency in handling image features, particularly in complex image structures [21], has been chosen. In this study, the reference data is very sparse in image, resulting in limitations in data quantity for deep learning training. Meanwhile, the U-Net model demonstrates its capacity for training with less training data and can learn spatial localization features, a critical aspect for achieving precision in predicting AGB at each pixel.

2.4.1 Data preparation for model development

For data sampling, the region in Thailand was randomly selected at random using discrete uniform sampling that does not contain NAN values from Sentinel-1 and Sentinel-2 and should have GEDI footprint data. Furthermore, the distribution pattern of all three of these data must be consistent. A total of 40,000 images were used for model development, and they were divided into three sets: a Training Set (85%), a Validation Set (15%) and a Test Set (15%). The Test Set was separated from the Validation Set. Data preparation for model development must not be duplicated and overlapping in terms of spatial information which prevents model bias during model accuracy evaluation. Data preparation involved random window sampling, images of 244 x 244 pixels were selected, which allows capturing the overall spatial details while maintaining computational feasibility.

2.4.2 Training procedures

The U-Net model was developed using the supervision approach by the Pytorch framework [22], where a deep ensemble technique was used to provide model uncertainty. The model's weights were randomly initialized in each candidate ensemble. Therefore, the models calculated loss only at the pixels with GEDI footprint by Gaussian negative log-likelihood function. For the model optimizer, ADAM was used to minimize the loss function during the training [23]. The data was divided into 32 batches and the learning rate size was adaptively adjusted using Cyclical "Triangular2" scheduling [18]. The learning rate began at 0.0000001 and reached a maximum of 0.1. The models were trained for 100 epochs, but Early Stopping technique was applied when no significant improvement was observed in the validation accuracy.

2.4.3 Uncertainty estimation

Despite deep learning methods having a high efficiency in accurately predicting outcomes, it can make highly confident predictions for input data it hasn't seen before [24][25]. For consideration using model outputs, models need to address uncertainty, classified into two types based on the uncertainty source [26], namely, 1. Aleatoric uncertainty that comes from the noise in training data. 2. Epistemic uncertainty from the model missing some of the information in training data [24]. Aleatoric uncertainty can measured directly form data by learning set of variances corresponding to the input, using Gaussian negative log likelihood (NLL) equation as outlined in Equation 1 [27] as the function to calculate loss from the training dataset [26].

$$\mathcal{L}_{NLL} = \frac{1}{N}\sum_{i=1}^{N}\frac{(\hat{\mu}(x_i) - y_i)^2}{2\hat{\sigma}^2(x_i)} + \frac{1}{2}\log\hat{\sigma}^2(x_i). \quad (1)$$

To evaluate Epistemic Uncertainty, we need to introduce some stochastic to the model, the approach involved constructing an ensemble model [24]. Here, five same models were created, each initialized with different random parameter values [22]. The uncertainty model was evaluated using the total variance formula (Equation 3). This formula combines both Epistemic Uncertainty terms (1 and 2) and Aleatoric Uncertainty terms (3). The AGB density result was calculated by averaging output from five models with the same weight (Equation 2) [27]. Fig. 4 illustrates the flow of ensemble modeling.

$$\hat{y} = \frac{1}{M}\sum_{m=1}^{M}\hat{\mu}_m \quad (2)$$

$$Var(\hat{y}) = \frac{1}{M}\sum_{m=1}^{M}\hat{\mu}_m^2 - \left(\frac{1}{M}\sum_{m=1}^{M}\hat{\mu}_m\right)^2 + \frac{1}{M}\sum_{m=1}^{M}\hat{\sigma}_n^2 \quad (3)$$

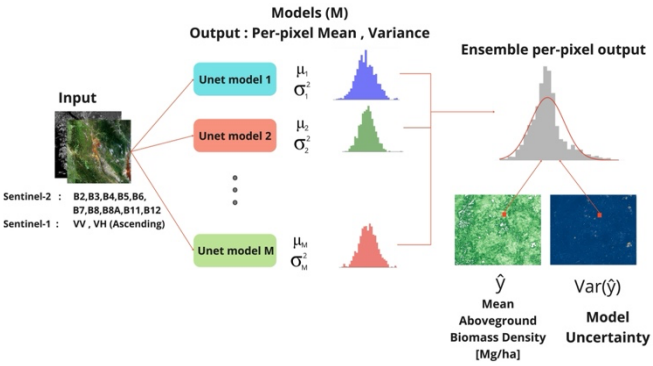

Fig. 4. Flow of ensemble modeling

3. RESULTS AND DISCUSSION

3.1 Test Set Validation

Testing with the GEDI Test Set, each model was evaluated and compared with ensemble prediction results as shown in Table 1, while Table 2 shows model evaluation using inventory data from T-VER-S-TOOL-01-01 Version 01 Carbon Storage Measurement Tool Annex announced by the Thailand Greenhouse Gas Management Organization (TGO) [28].

Table 1. Test set evaluation of the models

Model	RMSE (Mg/ha)	MAE (Mg/ha)
1	29.06	8.07
2	29.76	7.99
3	33.57	10.88
4	28.12	7.43
5	30.53	8.55
Ensemble	26.37	6.78

Table 2. Inventory data evaluation of the models

Plant / Forest type	Sample	MAE [kg/m²]	RMSE [kg/m²]	RRMSE (%)
Mixed Deciduous Forest	300	1.93	3.94	24.47
Dry Evergreen Forest	300	0.72	2.12	14.0
Pará rubber	283	1.45	3.33	17.05

3.2 Model Uncertainty Evaluation

Model uncertainty was evaluated by using a calibration plot for the predicted and GEDI Test Set [27]. Another crucial aspect for model uncertainty evaluation is assessing its performance on data outside the Training Set [29]. Calibration plot reveals that the majority of the predicted data trends closely with the reference data to a significant extent, indicating that the model has high confidence in accurate prediction. On the other hand, the model has low confidence in inaccurately prediction data as shown for low sample point and illustrated in Fig. 5.

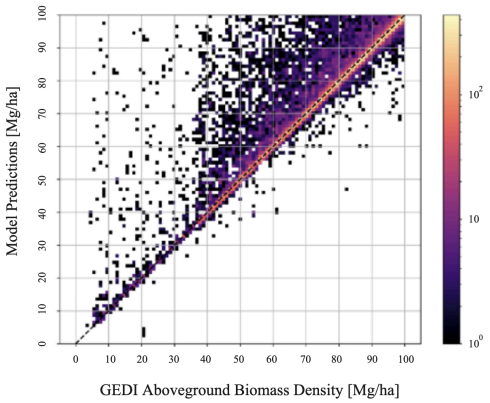

Fig 5. Ensemble model calibration plot

The model uncertainty assessment with out-of-distribution data involved comparing uncertainty from two areas which are dense forest area and urban or community area. The outcomes in the forest or wooded area corresponding to the training dataset exhibit a low standard deviation (SD). Conversely, out-of-distribution data areas exhibit a high standard deviation as shown in Fig. 6.

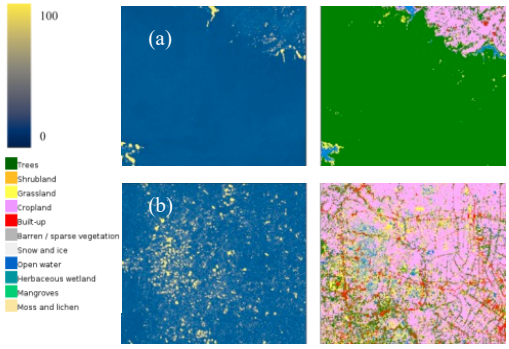

Fig 6. Uncertainty from ensemble models from
(a) similar distribution as training set (forest area)
(b) Out-of-distribution data area.

In conclusion, result show the potential of combining GEDI, Sentinel-1, Sentinel-2 EO data to advance methods for forest aboveground biomass estimation in Thailand albeit that the coverage of GEDI LiDAR footprint in Thailand is only partially cover. The uncertainty estimation result show that

the model can be improve by collecting more field inventory data for other forest species and considering areas that overlap with GEIDI sample to use as calibration data for improve accuracy of GEDI for using as reference target in model development. Another further improvement is to use more temporal range and implement time series model to cover every seasonal change in forest aspect.

4. REFERENCES

[1] L. Duncanson, J. R. Kellner, J. Armston, R. Dubayah, D. M. Minor, S. Hancock, et al., "Aboveground Biomass Density Models for NASA's Global Ecosystem Dynamics Investigation (GEDI) Lidar Mission," *Remote Sens. of Environ.*, vol. 270, 2022.

[2] R. Pedro, W. James, L. Valentin, T.Kevin, B. Heiko. "Quantifying Forest Biomass Carbon Stocks from Space," *Current Forestry Rep* 3.10.1007/s40725-017-0052-5, 2017.

[3] R. Dubayah, J. B. Blair, S. Goetz, L. Fatoyinbo, M. Hansen, S. Healey, et al., " The Global Ecosystem Dynamics Investigation: High-resolution laser ranging of the Earth's forests and topography," *Sci. of Remote Sens*., vol 1, 2020.

[4] M. Schwartz, P. Ciais, C. Ottlé, A. D. Truchis, C. Vega, I. Fayad, et al., "High-resolution Canopy Height Map in the Landes Forest (France) Based on GEDI, Sentinel-1, and Sentinel-2 Data with a Deep Learning Approach," *10.48550/arXiv.2212.10265*, 2022.

[5] R. Valbuena, B. O'Connor, F. Zellweger, W. Simonson, P. Vihervaara, M. Maltamo, et al., "Standardizing Ecosystem Morphological Traits from 3D Information Sources," *Trends in Ecology & Evolution*, vol. 35, Issue 8, pp. 656-667, 2020.

[6] N. Lang, K. Schindler, J. D. Wegner, "Country-wide High-resolution Vegetation Height Mapping with Sentinel-2," *Remote Sens. of Environ.*, vol. 233, 111347, 2019

[7] H. Ogawa, K. Yoda, K. Ogino, T. Kira, "Comparative ecological studies on three main types of forest vegetation in Thailand. II. Plant Biomass," *Nature and Life in Southeast Asia*, Flora and Fauna Res. Soc., vol. 4, pp. 49-80, 1965.

[8] T. Tsutsumi, K. Yoda, P. Sahunalu, P. Dhanmanonda, B. Prachaiyo, "Forest: Felling, Burning and Regeneration," *Shifting Cultivation,* pp. 13-62, 1983

[9] J. Hytönen, N. Kaakkurivaara, T. Kaakkurivaara, J. Nurmi, "Biomass Equations for Rubber Tree (Hevea brasiliensis) Components in Southern Thailand," *J. of Tropical Forest Sci.*, 30, pp. 588–596, 2018.

[10] M. Main-Knorn, B. Pflug, J. Louis, V. Debaecker, U. Müller-Wilm, F. Gascon, "Sen2Cor for Sentinel-2,", *3.10.1117/12.2278218.*, 2017.

[11] L. Huang, J. Qin, Y. Zhou, F. Zhu, L. Liu, L. Shao, "Normalization Techniques in Training DNNs: Methodology, Analysis and Application," arXiv:2009.12836, 2020.

[12] K. Soudani, N. Delpierre, D. Berveiller, G. Hmimina, G. Vincent, A. Morfin, E. Dufrêne, "Potential of C-band Synthetic Aperture Radar Sentinel-1 Time Series for the Monitoring of Phenological Cycles in a Deciduous Forest," *Int. J. Appl. Earth Obs. Geoinf.*, vol. 104, p. 102505, 2021.

[13] R.O Dubayah, J. Armston, J.R. Kellner, L. Duncanson, S.P. Healey, P.L. Patterson, et al., "GEDI L4A Footprint Level Aboveground Biomass Density, Version 2.1," ORNL DAAC, Oak Ridge, Tennessee, USA, 2022.

[14] J. R. Kellner, J. Armston, L. Duncanson, "Algorithm Theoretical Basis Document for GEDI Footprint Aboveground Biomass Density," *Earth and Space Sci.* 10.10.1029/2022EA002516. 2022.

[15] Y. Shendryk, "Fusing GEDI with Earth Observation Data for Large Area Aboveground Biomass Mapping," *Int. J. of Appl. Earth Observ. and Geoinformation,* vol. 115, 103108, 2022.

[16] A. Liu, X. Cheng, Z. Chen, "Performance Evaluation of GEDI and ICESat-2 Laser Altimeter Data for Terrain and Canopy Height Retrievals," *Remote Sens. Environ*., vol. 264, 112571, 2021.

[17] P. Potapov, X. Li, A. Hernandez-Serna, A. Tyukavina, M. C. Hansen, A. Kommareddy, et al., "Mapping Global Forest Canopy Height through Integration of GEDI and Landsat Data," *Remote Sens. Environ*., vol. 253, 112165, 2021.

[18] D. P. Roy, H. B. Kashongwe, J. Armston, "The Impact of Geolocation Uncertainty on GEDI Tropical Forest Canopy Height Estimation and Change Monitoring," *Sci. Remote Sens*., vol. 4, 100024, 2021.

[19] T. Watham, S. P. Kushwaha, S. Nandy, R. Patel, and S. Ghosh, "Forest Carbon Stock Assessment at Barkot Flux Tower Site (BFS) Using Field Inventory, Landsat-8 OLI Data and Geostatistical Techniques," *Int. J. of Multidisciplinary Res. and Develop.*, vol. 3, issue. 5, pp. 111-119, 2016.

[20] G. W. Pereira, D. S. M. Valente, D. M. de Queiroz, A. L. de F. Coelho, M. .M Costa, T. Grift., et al., "Smart-Map: An Open-Source QGIS Plugin for Digital Mapping Using Machine Learning Techniques and Ordinary Kriging," *Agronomy*, vol. 12, no.6, 1350, 2022.

[21] O. Ronneberger, P. Fischer, and T. Brox, "U-Net: Convolutional Networks for Biomedical Image Segmentation," *LNCS*, vol.9351, pp. 234-241, 2015.

[22] N. Lang, W. Jetz, J. Wegner, "A High-Resolution Canopy Height Model of the Earth," *Nature Ecology & Evolution*, vol.7, pp.1-12, 2023.

[23] D. Kingma and J. Ba, "Adam: A Method for Stochastic Optimization," arXiv:1412.6980*,* 2014.

[24] B. Lakshminarayanan, A. Pritzel, C. Blundell, "Simple and Scalable Predictive Uncertainty Estimation using Deep Ensembles," arXiv:1612.01474, 2017.

[25] C. Guo, G. Pleiss, Y. Sun, K. Q. Weinberger, "On Calibration of Modern Neural Networks," arXiv:1706.04599, 2017.

[26] A. Kendall, Y. Gal, "What Uncertainties Do We Need in Bayesian Deep Learning for Computer Vision," arXiv:1703.04977, 2017.

[27] N. Lang, N. Kalischek, J. Armston, K. Schindler, R. Dubayah, , J. D. Wegner, "Global Canopy Height Regression and Uncertainty Estimation from GEDI LIDAR Waveforms with Deep Ensembles," *Remote Sens. of Environ.*, vol. 268, 112760, 2022.

[28] Thailand Greenhouse Gas Management (Public Organization), "Tool for Calculation for Carbon Sequestration in tree under Thailand Voluntary Emission Reduction Program," 2023. [Online]. Available: https://ghgreduction.tgo.or.th/th/tver-method/tver-tool/for-agr/item/3451-calculation-for-carbon-sequestration.html

[29] S. Fort, J. Ren, B. Lakshminarayanan, "Exploring the Limits of Out-of-Distribution Detection," arXiv:2106.03004, 2021.